Supporting Information

Engineering the Photoresponse of Liquid-exfoliated 2D Materials by Size Selection and Controlled Mixing for Ultrasensitive and Ultraresponsive Photodetector

Fuad Indra Alzakia[1], Baoshan Tang[2], Stephen J. Pennycook[1], Swee Ching Tan[1]*

[1]Department of Materials Science and Engineering, National University of Singapore, 9 Engineering drive 1, Singapore 117574.

[2]Department of Electrical and Computer Engineering, National University of Singapore, 4 Engineering drive 3, Singapore 117583

Corresponding author e-mail: msetansc@nus.edu.sg

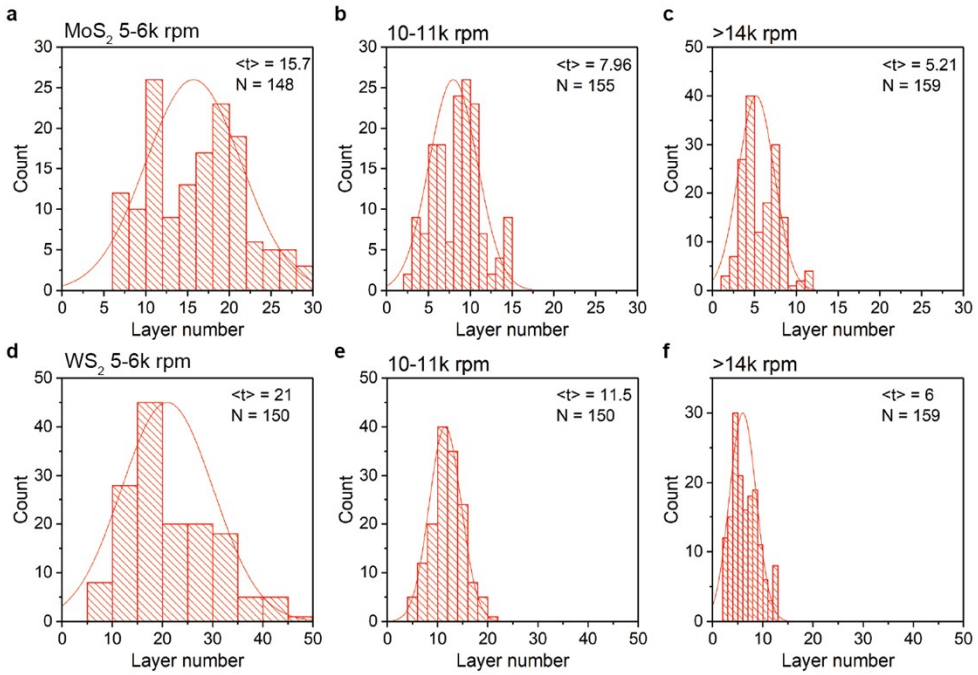

Fig. S1. Distribution of nanosheet layer numbers measured by AFM for MoS_2 and WS_2 dispersions obtained by (a, d) 5-6k rpm, (b, e) 10-11k rpm and (c, f) >14k rpm centrifugation windows. <t> is the average layer number, and N is the total number of nanosheets measured.

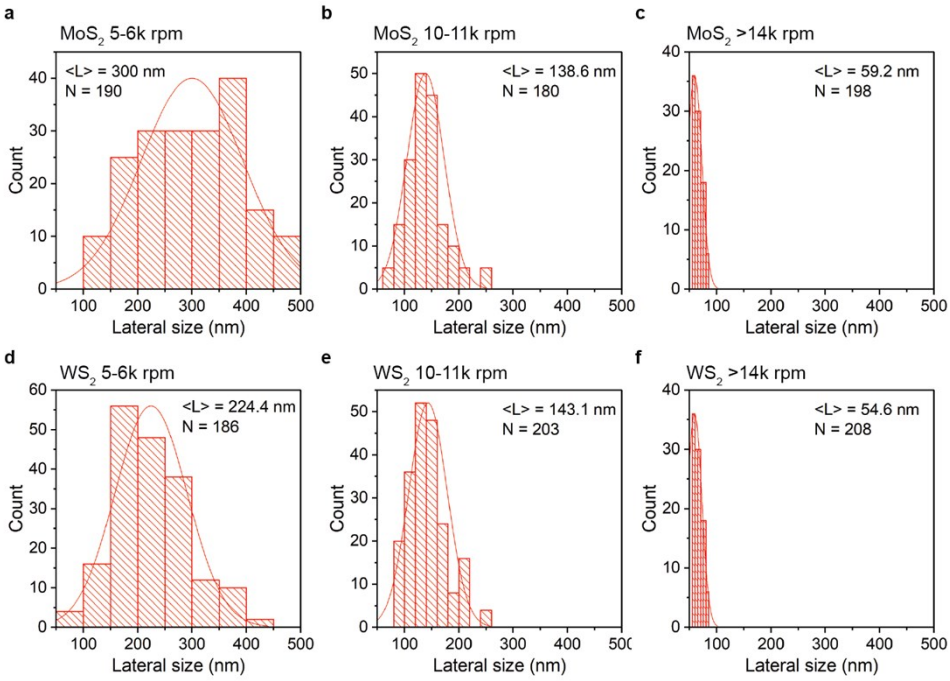

Fig. S2. Distribution of nanosheet lateral sizes measured by TEM for MoS_2 and WS_2 dispersions obtained by (a, d) 5-6k rpm, (b, e) 10-11k rpm and (c, f) >14k rpm centrifugation windows. <L> is the average lateral size, and N is the total number of nanosheets measured.

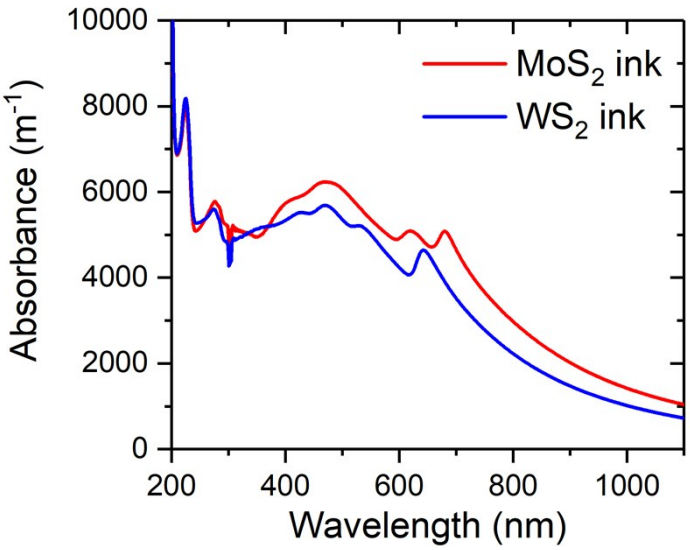

Fig. S3. UV-Vis absorbance spectra of the final MoS_2 and WS_2 inks with the concentration of 1.08 mg/ml and 1.26 mg/ml, respectively. Additional peaks at ~220 nm and ~280 nm are due to the added triton-x 100 in the final inks.

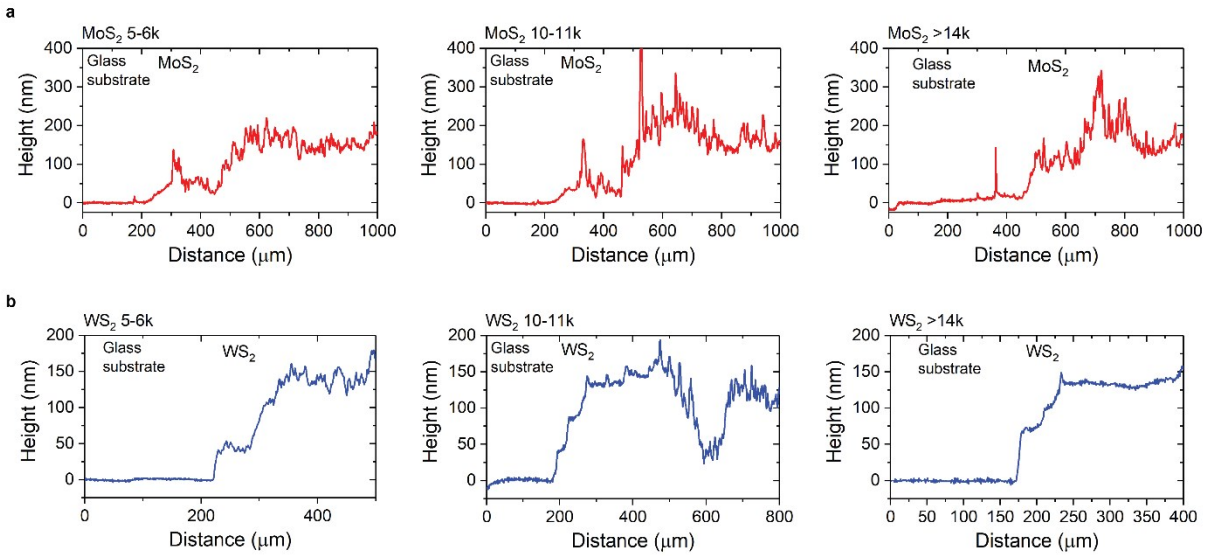

Fig. S4. Thickness profiles of (a) MoS_2 and (b) WS_2 photodetectors obtained from different centrifugation windows using surface profilometer.

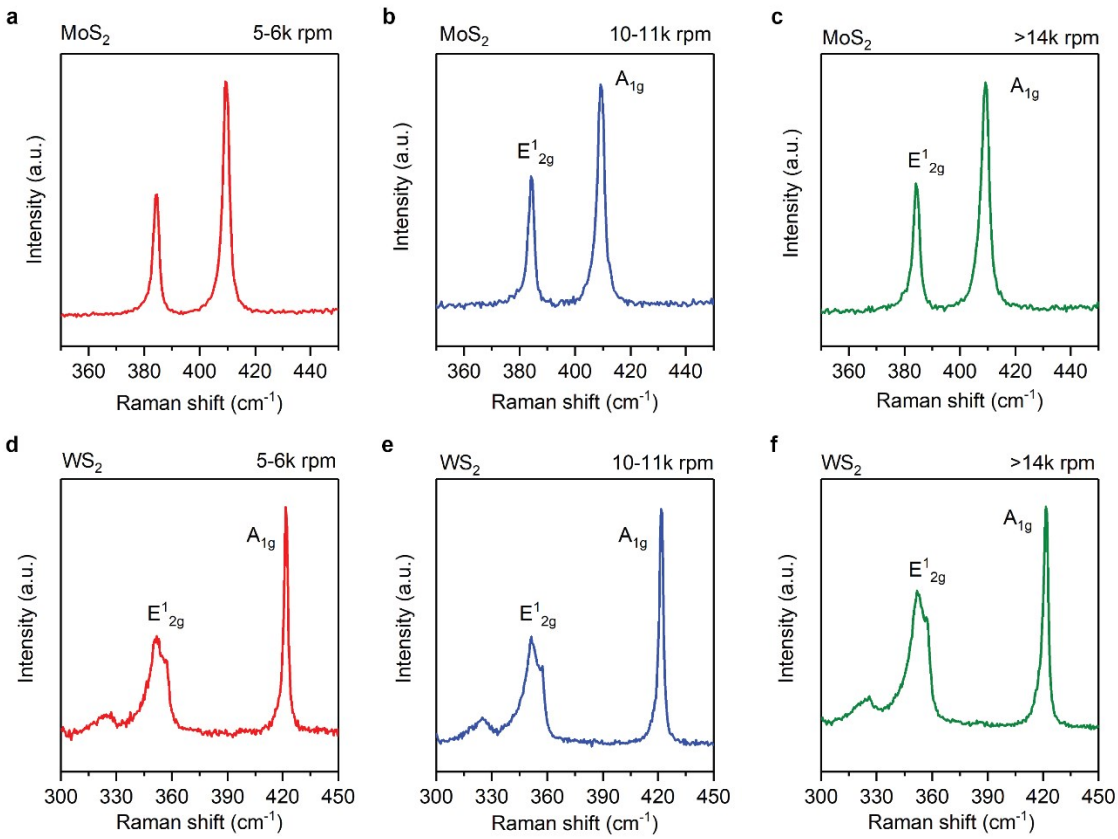

Fig. S5. Raman spectra of printed MoS_2 and WS_2 films obtained by centrifugation windows: (a,d) 5-6k rpm, (b,e) 10-11k rpm, and (c,f) >14k rpm.

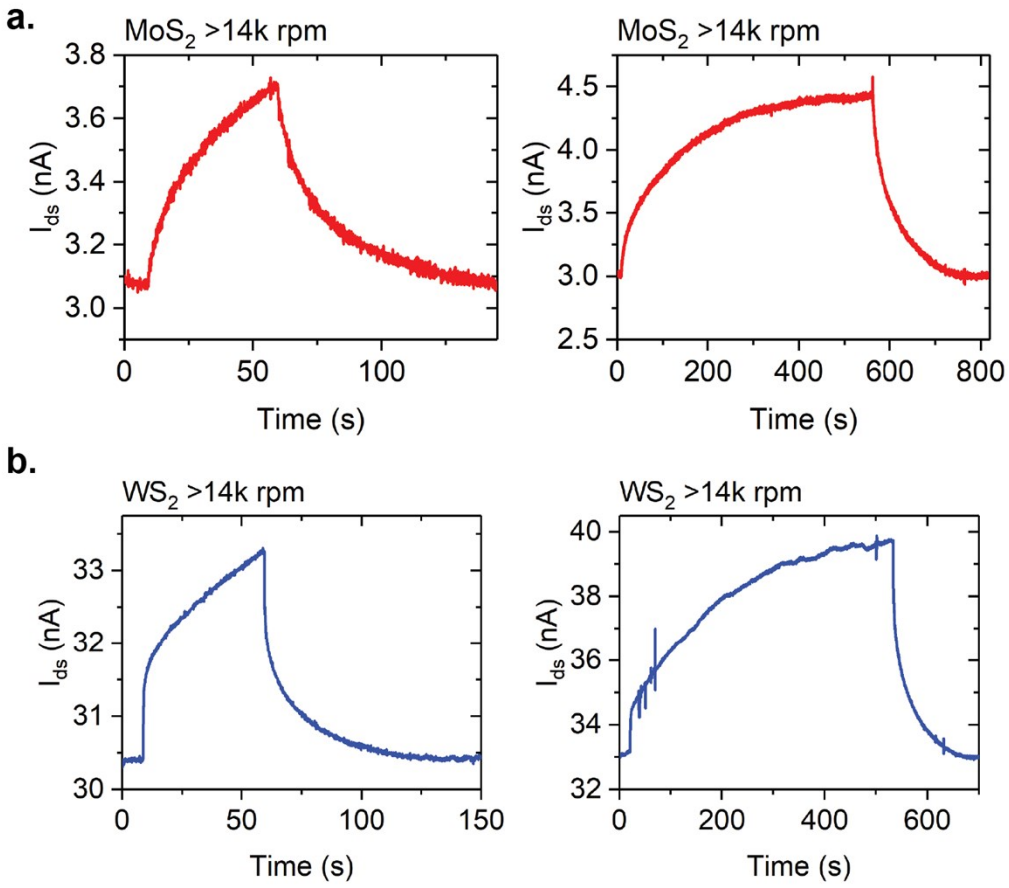

Fig. S6. Photocurrent transients of (a) MoS_2 and (b) WS_2 (>14k rpm) under 50 s illumination (left) and 500 s illumination (right). Persistent photocurrents are negligible even after prolonged (500 s) illumination, and the currents slowly return to the initial dark current state after switching off the illumination

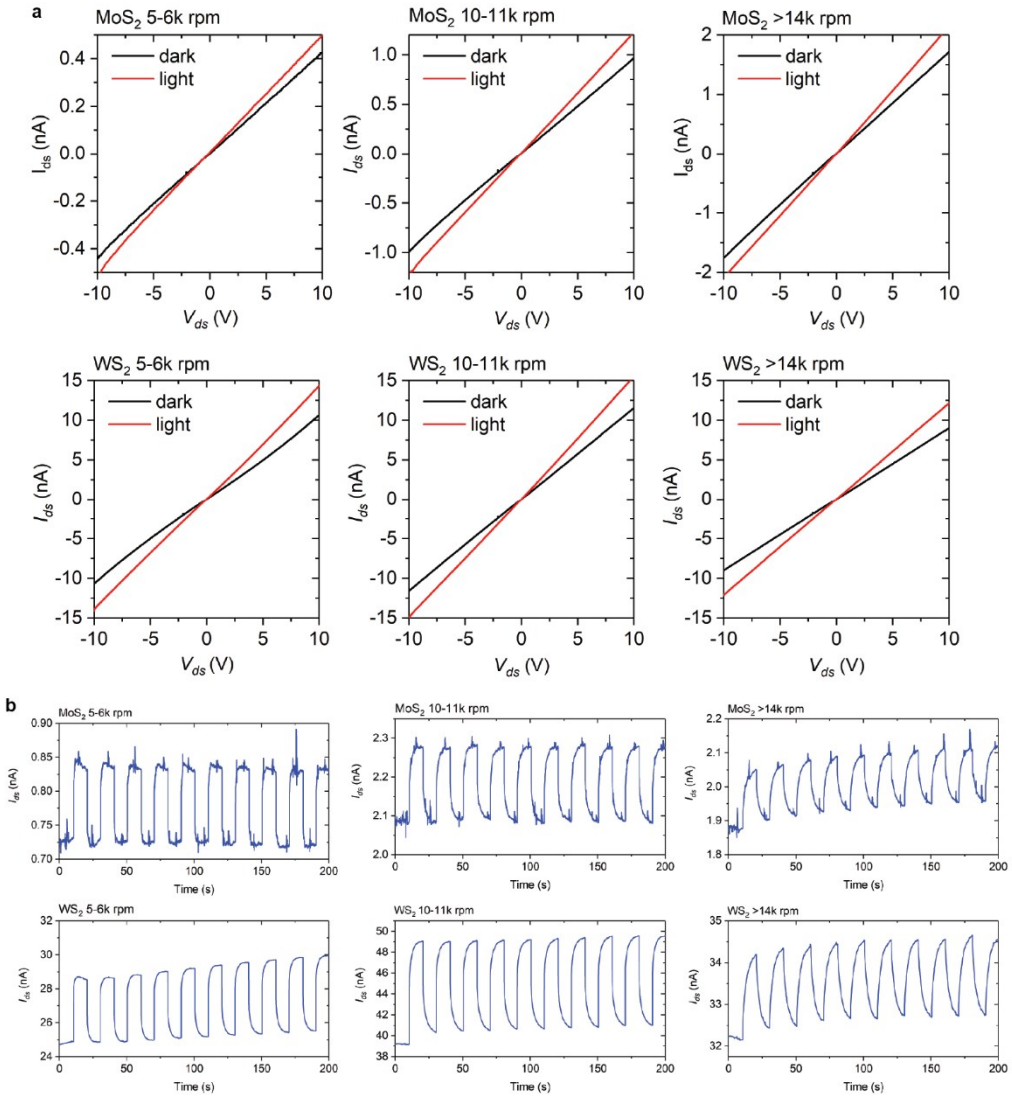

Fig. S7. (a) I_{ds}-V_{ds} plots of MoS_2 and WS_2 photodetectors fabricated from different centrifugation windows under dark and illuminated conditions (white light, 100mW/cm^2). (b)Photocurrent transients of MoS_2 and WS_2 photodetectors under multiple on-and-off light switching. V_{ds} =20 V.

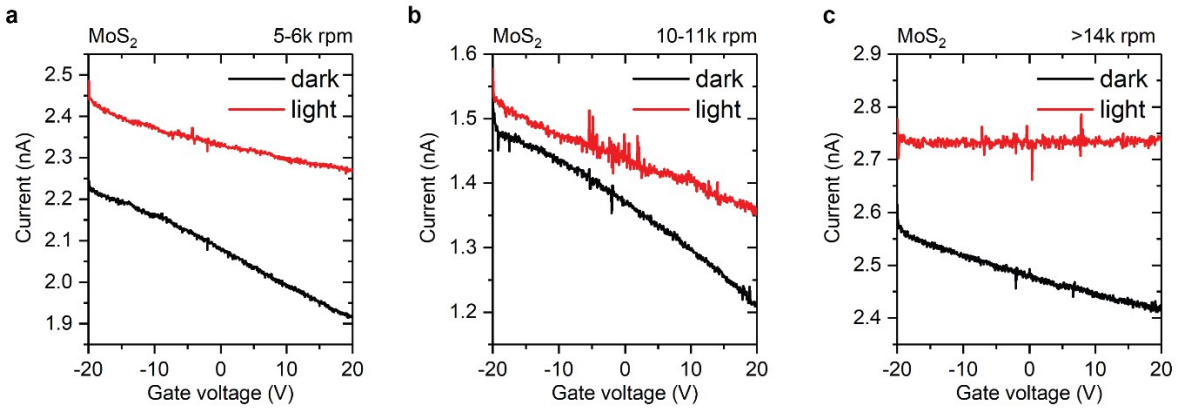

Fig. S8. Transfer curves of deposited MoS_2 photodetectors on Si/SiO_2 substrate obtained by centrifugation windows: (a) 5-6k rpm, (b) 10-11k rpm, and (c) >14k rpm, showing p-type behaviors. Under illumination, the modulation of current under gate bias becomes much weaker for >14k rpm centrifugation window, indicating the presence of stronger photogating effect compared to lower centrifugation windows.

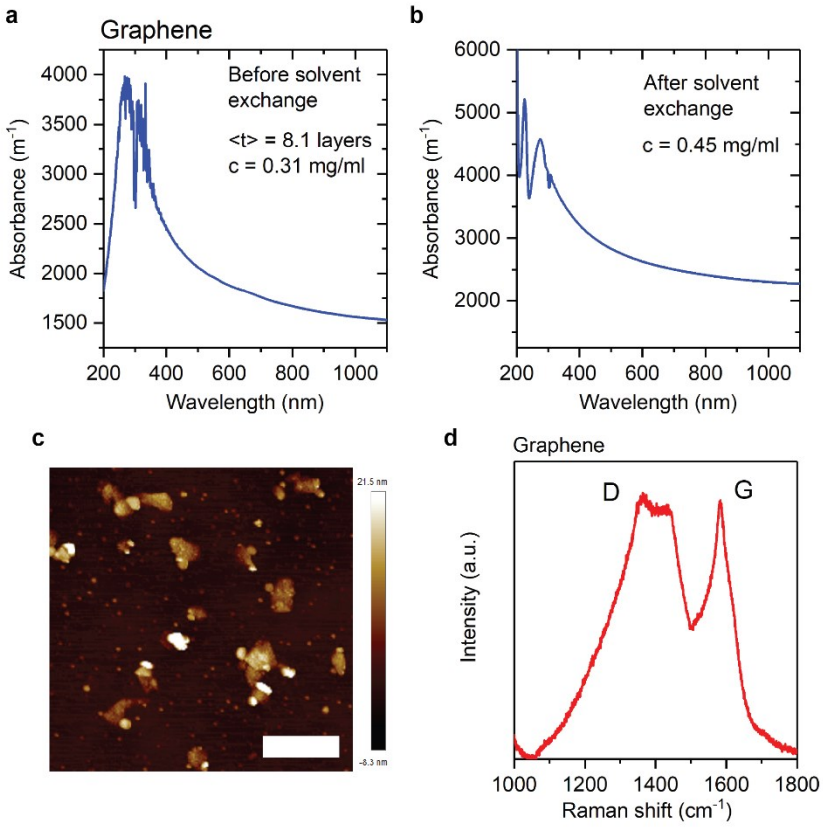

Fig. S9. (a) UV-Vis spectrum of graphene dispersion in isopropanol/water mixture right after exfoliation by bath sonication. The average layer number was 8.1 layers. (b) UV-Vis spectrum of graphene ink after solvent exchange to propylene glycol/water mixture used for printing. The additional peak at ~220 nm are from the added triton-x 100 to modify the surface tension of the ink. (c) AFM image of the graphene nanosheets. The lateral sizes are in the range of 100-300 nm, with many additional quantum dot-sized graphene. Scale bar: 500 nm. (d) Raman spectrum of the graphene dispersion.

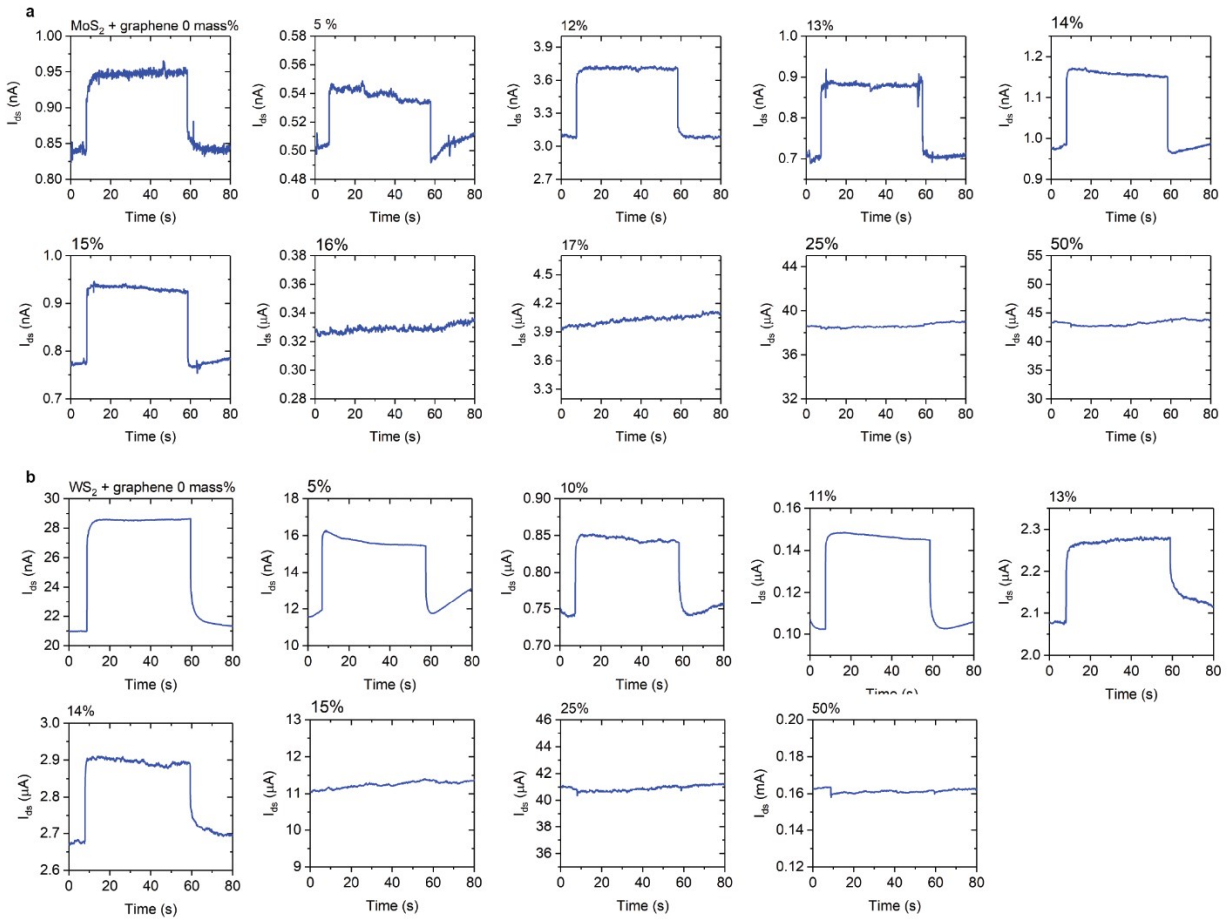

Fig. S10. Photocurrent transients of (a) MoS_2/graphene and (b) WS_2/graphene composite photodetectors as a function of graphene loadings in mass% under illumination of 100mW/cm^2 of white light. V_{ds} = 20 V.

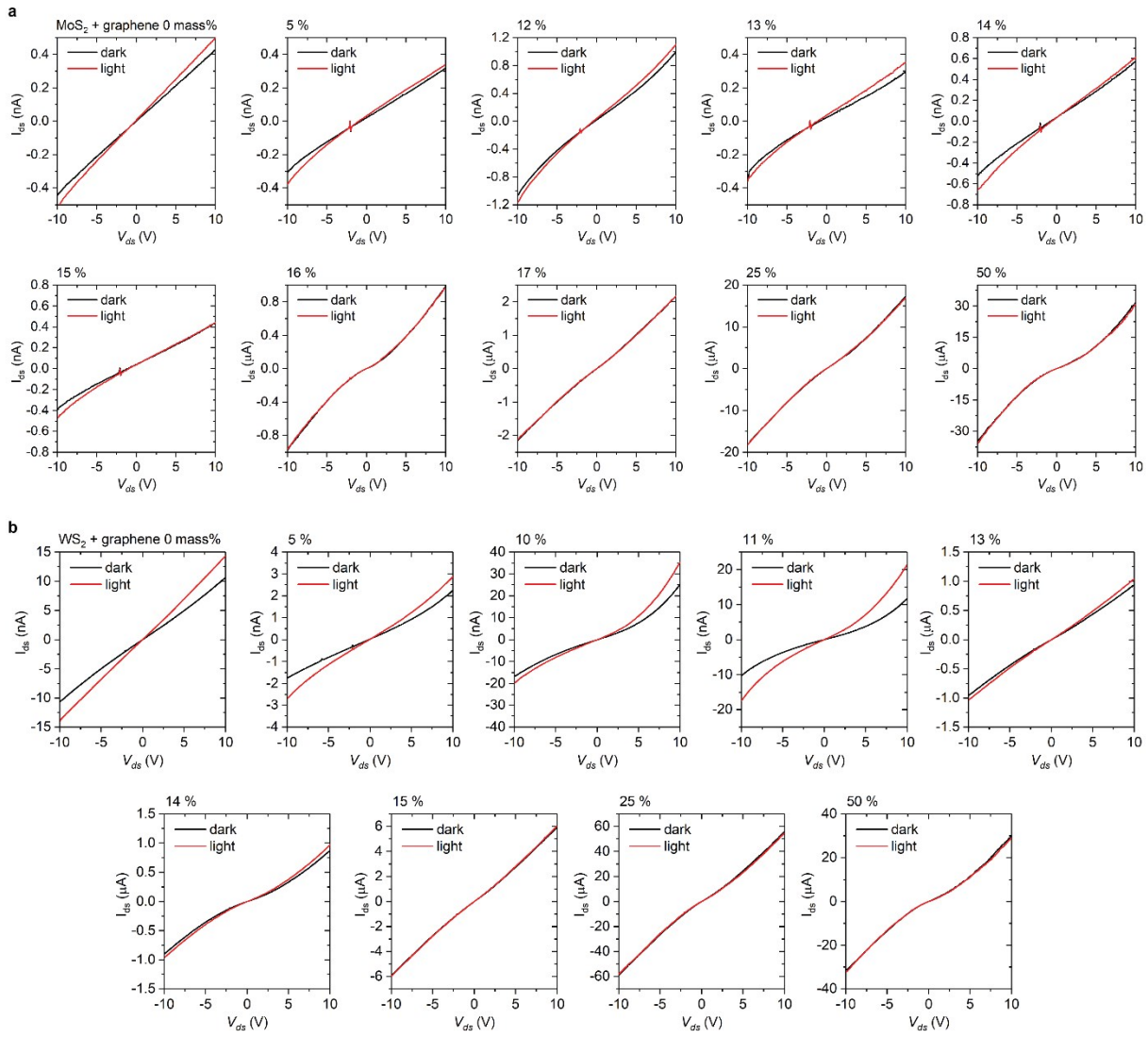

Fig. S11. I_{ds}-V_{ds} characteristics of (a) MoS_2/graphene and (b) WS_2/graphene photodetectors with different graphene mass% contents under dark and illuminated conditions (white light, 100mW/cm^2).

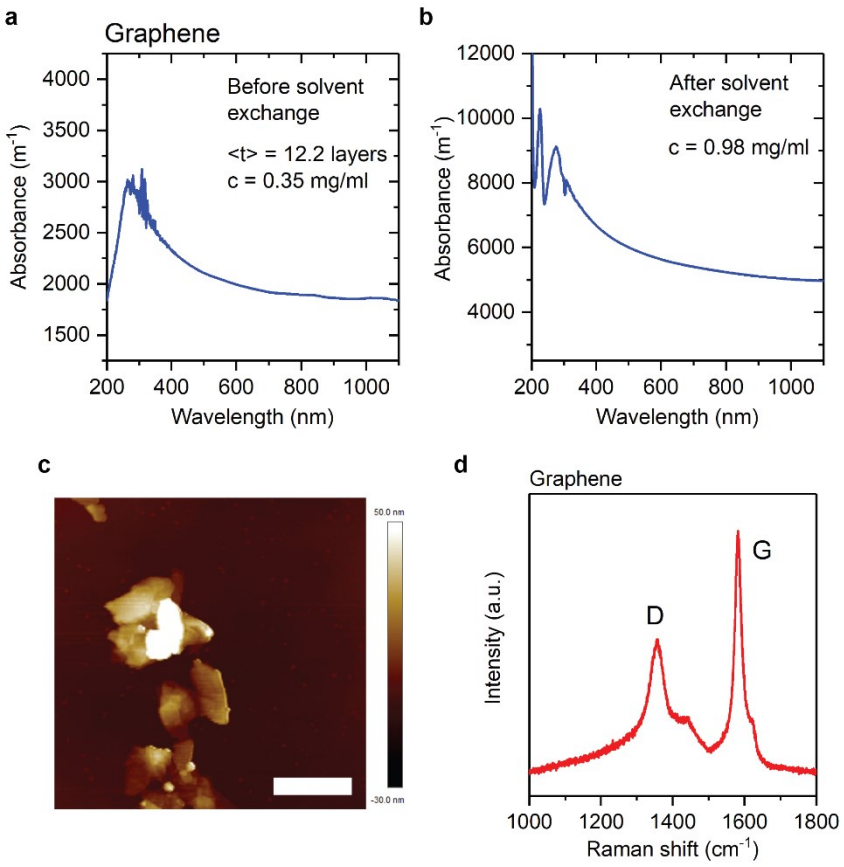

Fig. S12. (a) UV-Vis spectrum of graphene dispersion in isopropanol/water mixture right after exfoliation by bath sonication. The average layer number was 12.2 layers. (b) UV-Vis spectrum of graphene ink after solvent exchange to propylene glycol/water mixture used for printing. The additional peak at ~220 nm are from the added triton-x 100 to modify the surface tension of the ink. (c) AFM image of the graphene nanosheets. The lateral sizes are in the range of 300-500 nm. Scale bar: 500 nm. (d) Raman spectrum of the graphene dispersion.

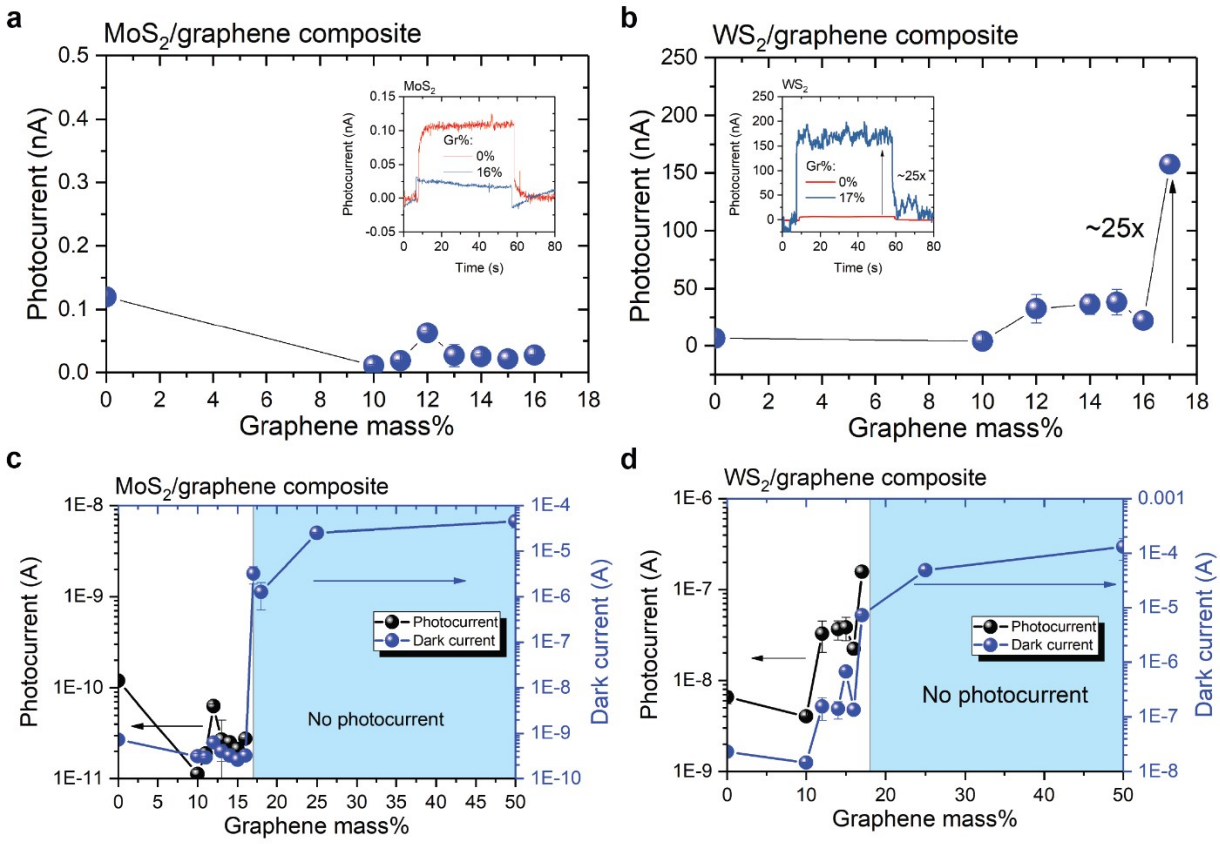

Fig. S13. MoS_2/graphene and WS_2/graphene composite photodetectors composed of graphene with larger average thickness (<t> = 12.2 layers). (a,b) Evolution of photocurrents for (a) MoS_2/graphene and (b) WS_2/graphene composite photodetectors as a function of graphene mass% loadings. The photocurrent increase of WS_2/graphene photodetector only reached ~25× compared to pure WS_2 photodetector. (c,d) the photocurrents as function of graphene mass% loadings superimposed with the dark currents of MoS_2/graphene (c) and WS_2/graphene photodetectors. Similar to the composite photodetectors with the thinner graphene, the photocurrent increase in only observed near the percolation threshold.

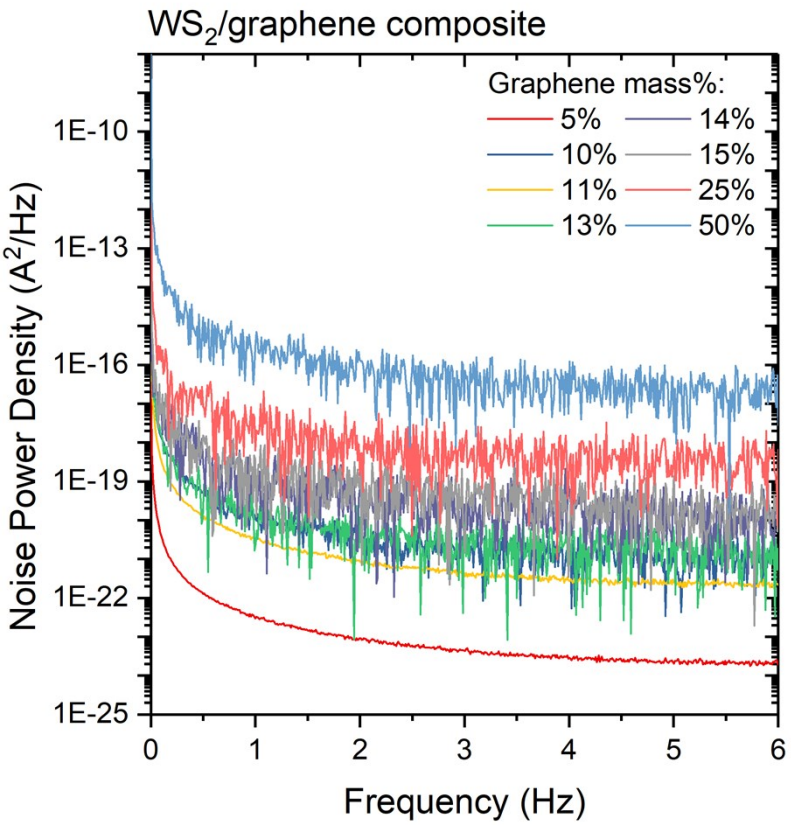

Fig. S14. The noise power density (NPD) spectrum of the dark currents of WS_2/graphene composite photodetector as a function of graphene mass% loadings. The NPDs were obtained by Fast Fourier Transfer (FFT) processing of the measured dark currents. The noise currents plotted in Fig. 4g were obtained by integrating the NPD spectra across the frequency range.

Supplementary note 1. Effect of the average nanosheet size in the network and dark conductivity.

As we see in Fig. 2b in the main manuscript, the dark current seems to increase as the average nanosheet size is reduced, which is counterintuitive given that more inter-nanosheet junctions are supposed to be formed as nanosheet size becomes smaller, which increases the junction resistance. We propose the following mechanisms that might lead to this interesting observation. First, different porosity (compactness) of the nanosheet network when the average nanosheet size is large versus small. Even though more inter-nanosheet junctions form in the nanosheet network with small average size, the network might be more compact (less porous) than large nanosheet network because small nanosheet size is easier to fill up empty spaces. Thus, the effective cross-section area of the conducting channel might be larger for the network of small nanosheets, reducing the resistance. On the other hand, due to the bulkier nature of large nanosheets, there might be more empty spaces between the nanosheets, reducing the effective cross-section area of the conducting channel, increasing the resistance. Second, different carrier concentration between small and large nanosheets. We expect the smaller nanosheets to be more susceptible to doping from the surrounding environment (residual solvent molecules, ambient gas, etc) compared to large nanosheets because injected carriers can penetrate the entire nanosheet volume more easily due to the small size. Since the conductivity is the product between the mobility and carrier concentration, it might be that small nanosheets have higher carrier concentration than larger nanosheets which more than compensates the reduction in mobility due to the increased inter-nanosheet junctions. Therefore, even though we are still not certain of the origin of the higher conductivity of small nanosheet network, the above proposed mechanism might explain the observation.

Supplementary note 2. Effect of material's bandgap, mobility, and carrier density on the magnitude of photocurrent.

Previous reports show that the bandgap of bulk MoS_2 and WS_2 are not very different, (~1.2-1.3eV), with WS_2 having slightly higher bandgap (~0.1 eV) than MoS_2.[1–3] We assume that majority of the nanosheets we obtained are in bulk form, since the average layer number obtained even under highest centrifuge speed (>14k rpm) is above 4 layers. Therefore, the bandgap difference is certainly not the origin of the large discrepancy of the magnitude of the photocurrents between MoS_2 and WS_2. On top of that, since the light used for the test was a broadband (white) light with 1-sun intensity, and the extinction coefficients of MoS_2 and WS_2 dispersion at the A-exciton peak for average nanosheet size of ~300 nm are roughly the same (~40 ml mg^{-1} cm^{-1}),[4,5] we estimate that the amount of photons absorbed per second is roughly similar between the two devices. Therefore, the bandgap and the optical properties of MoS_2 and WS_2 are likely not the origin of the large discrepancy in the photocurrents.

The larger photocurrent of liquid exfoliated WS_2 than MoS_2 by almost 2 orders of magnitude has also been reported by Cunningham et al.[6] In the paper, the author discovered that the ratio of photoconductivity σ_{ph} (σ_{total}-σ_{dark}) and dark conductivity σ_{dark} shows a clear exponential function versus the indirect bandgap of the material, E_g:

$$\frac{\sigma_{ph}}{\sigma_{dark}} \propto e^{\frac{E_g}{2kT}}$$

Interestingly, all of the TMD materials tested (MoS_2, $MoSe_2$, $MoTe_2$, WS_2, WSe_2, WTe_2) all fall roughly on the same curve. Since the bandgap of MoS_2 and WS_2 are almost the same,

$$\frac{I_{ph,MoS_2}}{I_{ph,WS_2}} = \frac{\sigma_{ph,MoS_2}}{\sigma_{ph,WS_2}} \approx \frac{\sigma_{dark,MoS_2}}{\sigma_{dark,WS_2}}$$

where I_{ph} is the photocurrent described in our manuscript. Surprisingly, we observed that the ratio I_{ph}/I_{dark} are also roughly similar between MoS_2 and WS_2, which is in the range of 0.1-0.3: 0.17±0.04 (MoS_2) and 0.29±0.07 (WS_2) for 5-6 krpm, 0.1±0.02 (MoS_2) and 0.23±0.05 (WS_2) for 10-11 k rpm, and 0.1±0.03 (MoS_2) and 0.13±0.02 (WS_2) for >14 k rpm.

Therefore, the photocurrents of MoS_2 and WS_2 photodetectors are roughly proportional to the magnitude of the dark currents. The ratios of the dark current between WS_2 and MoS_2 in our experiment are as follows: ~32 for 5-6 krpm, ~14 for 10-11 k rpm, and ~9 for >14 k rpm. Meanwhile, the dark conductivity σ_{dark} can be expressed as:[6]

$$\sigma_{dark} = \mu e N_c e^{-\frac{E_g}{akT}}$$

where μ is the mobility, N_c is the effective density of states in the conduction band, and a is a constant that depends on the doping of the material (2 for intrinsic semiconductor). Since the bandgap of MoS_2 and WS_2 are almost the same, we can assume that the exponential component is similar between MoS_2 and WS_2. Therefore, the large discrepancy between the dark currents of MoS_2 and WS_2 is largely determined by the difference of the product of mobility μ and N_c between the two materials.

According to previous reports, the mobility of WS_2 is roughly 2x that of MoS_2 either in a single nanosheet[7] or in a network.[8] The product of N_c and $e^{-Eg/akT}$ is the dark carrier concentration n, due to thermal activation. According to previous report, the carrier concentration of a dry network of WS_2 nanosheets are approximately 10 times that of MoS_2 nanosheets (2.6×10^{13} cm^{-3} for WS_2 versus 2.1×10^{12} for MoS_2).[8] Therefore, according to this calculation, the dark current of WS_2 should be ~2×10 =~20 times larger than the dark current of MoS_2, which is in a fairly good agreement with our observation (between 9 to 32 times).

And, as we have mentioned above, the magnitude of the photocurrent roughly follows the magnitude of the dark current.

Therefore, even though the above calculation is rather simplified, we can see that there are a complex interplay between different physical quantities which determines the magnitude of the photocurrent, which are the material's bandgap, mobility, and the effective density of states of the material.

Supplementary note 3. Effect of mobility differences on the response times

In our experiment, all of the photodetectors we fabricated have similar channel length, which is 1 mm. therefore, we can exclude the variability of response times due to varying channel lengths. Regarding the dependence on mobility, we expect the mobility to change depending on the average nanosheet size, where smaller average nanosheet size would result in lower mobility because more inter-nanosheet junctions are formed, which increase the total resistivity. The mobility of the nanosheet network can be approximated to be proportional to the average nanosheet size:[9]

$$\mu \propto \frac{1}{\rho} \propto d$$

where μ is mobility, ρ is the resistivity, and d is the average nanosheet size. The mobility of MoS_2 and WS_2 networks with average nanosheet size of ~300 nm has been reported to be ~0.1 cm^2/Vs.[8] Since the average nanosheet size for 5-6k rpm is ~250 nm and for >14k rpm is ~50 nm in our manuscript, we can approximate the mobility for MoS_2 and WS_2 networks with average small size to be:

$$\mu_{small} \approx \frac{d_{small}}{d_{large}} \times \mu_{large} = \frac{50}{250} \times 0.1 = 0.02 cm^2 / Vs$$

The response time due to channel mobility is equivalent to transit time τ_t, which can be expressed as:

$$\tau_t = \frac{l}{v}$$

where l is the channel length and v is the carrier velocity. v can be expressed as:

$$v = \mu E = \mu \frac{V_{ds}}{l}$$

Where E is the electric field and V_{ds} is the source-drain voltage. The V_{ds} applied in the experiment is 20V. Therefore, the transit time can be calculated as:

For large nanosheets:

$$\tau_t = \frac{l}{v} = \frac{l^2}{\mu V_{ds}} = \frac{\left(1\times10^{-3}\right)^2 m^2}{1\times10^{-5} m^2/V\cdot s\times 20V} = 5\times10^{-3} s$$

For small nanosheets:

$$\tau_t = \frac{l}{v} = \frac{l^2}{\mu V_{ds}} = \frac{\left(1\times10^{-3}\right)^2 m^2}{2\times10^{-6} m^2/V\cdot s\times 20V} = 25\times10^{-3} s$$

Since the response time for large nanosheets is ~2 s and for small nanosheets is ~30 s in our manuscript, we can safely ignore the component of the response time due to different transit times and thus, due to different mobility. Therefore, in our manuscript, we solely focus our investigation on the effect of carrier lifetimes on the response time due to carrier trapping at the edge sites.

Supplementary note 4. Photogating effects from ink residues, gas adsorbates, and substrate.

Since the photocurrent measurements were all performed in air, the charge stored in adsorbates such as oxygen and water can also cause surface states to form and cause band bending at the nanosheet surface, as has been reported elsewhere.[10,11] The edge states might not entirely originate from defect states due to dangling bonds but might also be the result of adsorbed gas molecules from the air. Even though gas molecules can also adsorb on the basal planes of the nanosheets, we mainly focus on the edge sites because they have higher surface energy than basal planes due to dangling bonds, thus they are expected to interact more strongly with gas adsorbates than the basal planes. Therefore, we believe that the edge sites have a much more important role as carrier trapping centers that cause photogating effect compared to basal planes. Thus, in the simplified numerical model that we developed, we assume that carriers are trapped only at the edge sites, but not on the basal planes, to avoid complex calculations.

Other than gas adsorbates, residues from the ink formulations such as solvents, surfactants, and binder molecules that remain in the network and in contact with the nanosheets can also cause surface states to form and trap carriers. But all of the devices tested in our experiments (5-6k rpm, 10-11k rpm, and >14k rpm) were printed from similar ink formulations, that is, all the inks contained the same solvents with the same amount of surfactants and additives, and all of them were subjected to similar annealing conditions. Therefore, all of the devices should contain roughly similar solvent residues in the networks. Therefore, we believe that the photogating effect from the residues, if it exists, is not the main origin of the large variation of response times observed from devices made from nanosheets with different average sizes.

Regarding the interface with the glass substrate, it is also possible that charge trapping can occur at the nanosheet-substrate interface, causing photogating, as has been reported elsewhere.[12] However, since only

nanosheets at the bottom layer that are in contact with the substrate, we believe that the effect is minimal. For example, as the largest average nanosheet thickness obtained was ~20 layers (Fig. 1e in main manuscript), which corresponds to thickness of ~12 nm, and the typical total thickness of the device is ~100-200 nm (Fig. S4), thus, only up to ~6-12% of the device volume is affected by the substrate. Moreover, since the electrodes are contacted to the nanosheet network from the top, we believe that large proportions of the photocurrents are actually flowing within the top portions of the device. Also, all of the devices were deposited on the same glass substrate, therefore, we believe the large response time variations observed across different average nanosheet sizes were not originated from the photogating effect from the glass substrate.

Supplementary note 5. Role of the WS_2/graphene composite mobility on the photocurrent increase

The mobility increase of a network of WS_2 and graphene composite has been reported previously by O'suilleabhain et al.[13] In the paper, the mobility increase follows roughly the trend of conductivity increase of the composite as a function of graphene volume fraction (Fig. S15).

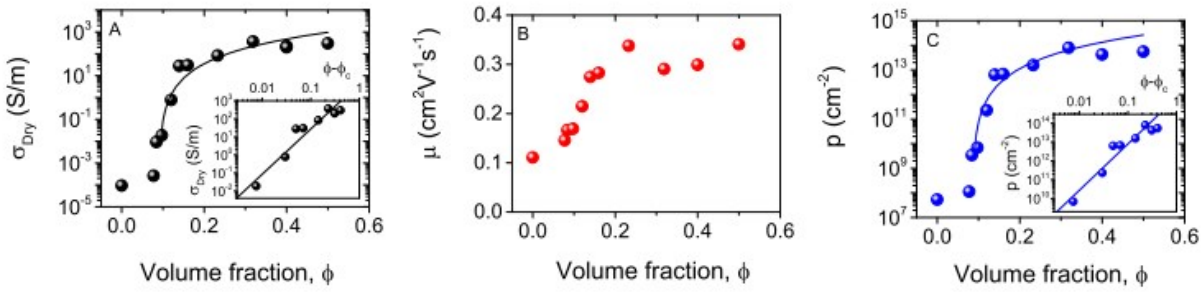

Fig. S15. (a) Conductivity of the WS_2 network (before the addition of IL), σ_{Dry}, vs graphene volume fraction. As the porosity of the deposited film is 0.5, the possible maximum graphene volume fraction is 0.5. (b) Hole mobility and (c) hole density (in the absence of IL) plotted vs graphene volume fraction. Note that the calculation of carrier density relies on the assumption that the mobility is the same with and without IL. Reproduced with permission.[13] Copyright © 2019 American Chemical Society.

In our manuscript, the magnitude of the photocurrent of WS_2/graphene composites follows roughly the magnitude of the dark current increase as it approaches the percolation threshold, and reaches its maximum at 14 mass% graphene, and suddenly disappears at the percolation threshold, at 15 mass% graphene. Using Equation 13 in our main manuscript, 14 mass% graphene corresponds to volume fraction of 0.18, and according to Fig. S15b, the mobility of the WS_2/graphene composite at 14 mass% graphene is ~0.3 cm^2/V.s, a ~3x increase from pure WS_2.

However, in our experiment, we observed a ~40x increase in the photocurrent at 14 mass% graphene compared to pure WS_2, even though the mobility increase is only ~3x increase (Fig. 4b). Therefore, the mobility increase alone might not be sufficient to explain the magnitude of the photocurrent increase. Even though we are not clear at this stage, we propose few possible explanations:

1. The author above assumes that the mobility of the WS_2/graphene composite network is the same whether in the wet state (soaked in ionic liquid) and in dry state.[13] Note that measurement of field effect mobility by transfer curve measurement is difficult for nanosheet network in dry state, due to weak capacitive coupling between the gate and the porous nanosheet network. Adding ionic liquid to the network significantly increases the capacitance between the gate and nanosheet, increases the on/off ratio, making the extraction of mobility easier.[8] Therefore, it is possible that the mobility in the dry state is actually different from the wet state. Since the ionic liquid acts more like a capacitor than a conductor, the addition of ionic liquid might increase the junction resistivity between nanosheets. Therefore, the actual mobility of the WS_2/graphene composites in the dry state might actually be higher than the above values.
2. As the photocurrent charge transfer occurs between WS_2 and graphene during illumination, photogating effect might also take place which increases the charge carrier concentration in the percolating graphene networks, which might also contribute to the increase in the photocurrent. For example, as shown in Fig. S16, if we assume that WS_2 is p-type, and photogenerated electrons are transferred to graphene during illumination while photogenerated holes remain in WS_2, the effective positive charges in WS_2 increases the electron concentration in the graphene network, increasing the photocurrent. Therefore, the photocurrent increase may not be only due to the mobility increase but also due to carrier concentration increase due to photogating effect at WS_2/graphene interface during illumination.

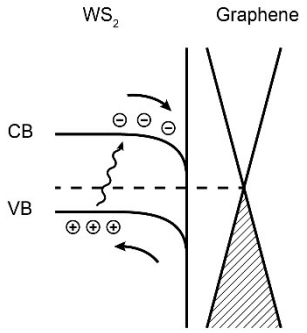

Fig. S16. Schematic of photogenerated charge transfer between WS_2 and graphene. The positively charged holes in WS_2 can cause photogating effect on the graphene network.

Therefore, there may be multiple factors that contribute to the increase in the photocurrent of WS_2/graphene composite at the percolation threshold, and we believe that the increase in the composite mobility at the percolation threshold, although may not be the sole factor, also plays a role in the increase in the photocurrent.

Supplementary note 6. Photogating effect in WS_2/graphene composite photodetector.

As we can see in Fig. 6b and d, sublinear relationship was observed between the magnitude of the photocurrent I_{ph} and the light power density P, in which the exponential factors are 0.22 and 0.35 for blue and green light, respectively. This is a clear indication that a photogating effect is taking place, as has been reported before.[14] However, as can be seen from the photocurrent transients of WS_2/graphene composite photodetectors in Fig. 6a, Fig. 6c, and Fig. S10, the response times are quite fast ($\leq$ 1 s), which are comparable to pure MoS_2 and WS_2 photodetectors obtained from 5-6k rpm centrifugation window (Fig. 2b). From the photocurrent transient data alone, the photogating effect seems to be almost absent. However, since the time resolution of our source meter is ~0.05 s, we cannot detect variations in the response time below ~0.05 s. Therefore, it is possible that the slowing down of photocurrent response time due to photogating effect caused by carrier trapping/de-trapping might occur, but we just could not detect it just by looking at the photoresponse transient data. However, the very low exponential factor in the relationship between I_{ph} and P ($<<1$) indicates that a strong photogating effect is actually occurring. Therefore, it is possible that in the case of WS_2/graphene mixture, the carrier trapping levels are of the shallow type, where the process of trapping and de-trapping of photoexcited carriers can happen almost instantaneously. As to the source of the photogating effect, it is likely that the small graphene nanosheets in the mixture (we can see large number of quantum dot sized graphene in AFM image in Fig. S9) are where the charge trapping might occur. We are doubtful that WS_2 nanosheets are the source of the photogating effect, since the nanosheet sizes are large (average size = 224.4 nm, see Fig. S2, obtained from 5-6k rpm centrifugation window), and the photogating effect has been shown to be absent in the pure WS_2 photodetector with large average nanosheet (Fig.2).

References

1. Wang, Q. H., Kalantar-Zadeh, K., Kis, A., Coleman, J. N. & Strano, M. S. Electronics and optoelectronics of two-dimensional transition metal dichalcogenides. *Nat. Nanotechnol.* **7**, 699–712 (2012).

2. Mak, K. F., Lee, C., Hone, J., Shan, J. & Heinz, T. F. Atomically thin MoS2: A new direct-gap semiconductor. *Phys. Rev. Lett.* **105**, 136805 (2010).

3. Zeng, H. *et al.* Optical signature of symmetry variations and spin-valley coupling in atomically thin tungsten dichalcogenides. *Sci. Rep.* **3**, 1608 (2013).

4. Backes, C. *et al.* Edge and confinement effects allow in situ measurement of size and thickness of liquid-exfoliated nanosheets. *Nat. Commun.* **5**, 4576 (2014).

5. Backes, C. *et al.* Production of highly monolayer enriched dispersions of liquid-exfoliated nanosheets by liquid cascade centrifugation. *ACS Nano* **10**, 1589–1601 (2016).

6. Cunningham, G., Hanlon, D., McEvoy, N., Duesberg, G. S. & Coleman, J. N. Large variations in both dark- and photoconductivity in nanosheet networks as nanomaterial is varied from MoS_2 to WTe_2. *Nanoscale* **7**, 198–208 (2015).

7. Jin, Z., Li, X., Mullen, J. T. & Kim, K. W. Intrinsic transport properties of electrons and holes in monolayer transition-metal dichalcogenides. *Phys. Rev. B - Condens. Matter Mater. Phys.* **90**, 045422 (2014).

8. Kelly, A. G. *et al.* All-printed thin-film transistors from networks of liquid-exfoliated nanosheets. *Science (80-.).* **356**, 69–73 (2017).

9. Zeng, H. *et al.* Grain size-dependent electrical resistivity of bulk nanocrystalline Gd metals. *Prog. Nat. Sci. Mater. Int.* **23**, 18–22 (2013).

10. Soci, C. *et al.* ZnO nanowire UV photodetectors with high internal gain. *Nano Lett.* **7**, 1003–1009 (2007).

11. Prades, J. D. *et al.* The effects of electron-hole separation on the photoconductivity of individual metal oxide nanowires. *Nanotechnology* **19**, 465501 (2008).

12. Zhang, K. *et al.* A substrate-enhanced MoS2 photodetector through a dual-photogating effect. *Mater. Horizons* **6**, 826–833 (2019).

13. O'suilleabhain, D., Vega-Mayoral, V., Kelly, A. G., Harvey, A. & Coleman, J. N. Percolation Effects in Electrolytically Gated WS_2/Graphene Nano:Nano Composites. *ACS Appl. Mater. Interfaces* **11**, 8545–8555 (2019).

14. Fang, H. & Hu, W. Photogating in Low Dimensional Photodetectors. *Adv. Sci.* **4**, 1700323 (2017).